2023

Design and Fabrication of Volume Holographic Optical Couplers for a Range of Non-Normal Incidence Angles

Dipanjan Chakraborty

Rosen Georgiev

Sinead Aspell

See next page for additional authors

Funder: Dipanjan Chakraborty is funded by Technological University Dublin Research Scholarship programme. Rosen Georgiev and Suzanne Martin received funding from Enterprise Ireland and the European Union's Horizon 2021 Research and Innovation Programme under the Marie Skłodowska-Curie grant agreement No. 847402. All authors thank FOCAS, TU Dublin for the provided technical facilities and administrative support.

Authors
Dipanjan Chakraborty, Rosen Georgiev, Sinead Aspell, Izabela Naydenova, and Suzanne Martin

Design and fabrication of volume holographic optical couplers for a range of non-normal incidence angles

Conference Paper · May 2023

DOI: 10.1117/12.2665596

7 authors, including:

Dipanjan Chakraborty
TU Dublin
3 PUBLICATIONS **5** CITATIONS
SEE PROFILE

Rosen Georgiev
TU Dublin
21 PUBLICATIONS **81** CITATIONS
SEE PROFILE

Vincent Toal
TU Dublin
155 PUBLICATIONS **2,222** CITATIONS
SEE PROFILE

Izabela Naydenova
TU Dublin
193 PUBLICATIONS **3,044** CITATIONS
SEE PROFILE

PROCEEDINGS OF SPIE

SPIEDigitalLibrary.org/conference-proceedings-of-spie

Design and fabrication of volume holographic optical couplers for a range of non-normal incidence angles

Dipanjan Chakraborty, Rosen Georgiev, Sinead Aspell, Vincent Toal, Izabela Naydenova, et al.

Dipanjan Chakraborty, Rosen Georgiev, Sinead Aspell, Vincent Toal, Izabela Naydenova, Dervil Cody, Suzanne Martin, "Design and fabrication of volume holographic optical couplers for a range of non-normal incidence angles," Proc. SPIE 12574, Holography: Advances and Modern Trends VIII, 125740E (31 May 2023); doi: 10.1117/12.2665596

SPIE.

Event: SPIE Optics + Optoelectronics, 2023, Prague, Czech Republic

Design and Fabrication of Volume Holographic Optical Couplers for a Range of Non-Normal Incidence Angles

Dipanjan Chakraborty [1,2], Rosen Georgiev [1,2], Sinead Aspell [1,2], Vincent Toal [1,2], Izabela Naydenova [1,2], Dervil Cody [1,2], Suzanne Martin [1,2]

[1] Centre for Industrial and Engineering Optics, School of Physics, Clinical and Optometric Sciences, TU Dublin, Grangegorman, Ireland.
[2] FOCAS Research Institute, TU Dublin, 13 Camden Row, Ireland.
* Correspondence: suzanne.martin@tudublin.ie.

1. ABSTRACT

A theoretical model has previously been developed to calculate the holographic recording beam angles required in air (at any recording wavelength) to produce a Volume Holographic Optical Element (VHOE) for operation as a coupler for different input and output angles. In this paper, the experimental study is extended to further validate the VHOE coupler design and fabrication approach for additional incident beam angles, comparing -40° -45° and -50° (in air). The output angle for each VHOE is +45° within the medium and the coupler operational wavelength is 633nm. Holographic recording in Bayfol HX 200 photopolymer at 532nm is used to fabricate the VHOE couplers. The experimental Bragg curves for each VHOE coupler obtained at 633 nm demonstrate agreement of the measured angles to within ±1.5° (in air) with the expected values.

Keywords: holography, holographic coupler, waveguide, non-normal incidence, Bayfol, volume holography, spurious gratings, HOE, VHOE, diffraction

2. INTRODUCTION

Holographic optical elements (HOEs) are of increasing importance in fields such as augmented reality, LED light shaping and solar collection, where their transparency off-Bragg can be as important a feature as their high efficiency on Bragg. Increasingly there is a need to develop the ability to design systems with specific central incident and diffracted angles, high Diffraction Efficiency and optimized wavelength selectivity. Since HOEs are holograms whose purpose is to replicate the function of optical components such as mirrors, lenses, etc., they have great potential to find application as functional optical films and coatings, but to do so they must be relatively low cost to produce. Volume HOEs have been developed for a broad range of applications including data storage (1),(2),(3) optical communication(4), (5), (6), (7), (8) and others (9), (10) but two of the most active research areas in recent years have been augmented reality displays and solar concentrators.

Augmented reality (AR) displays combine a digital image with the real world view, capitalizing on the transparency of HOEs when illuminated off-Bragg so that the image can be overlaid on the real world around the viewer (11); head-up displays (HUDs) and head mounted displays (HMDs) have typical fields of view (FOVs) of 30° and 45° respectively (12). HOEs have been used as part or all of the optical system. For example, Li et al. created a holographic augmented reality display using a mirror-lens HOE (13) and Piao et al. fabricated full colour HOEs to replace both the couple-in and couple-out optics in the head-mounted display(14). Whereas in (15), which involved a waveguide-based system, a prism was used as in coupler and reflective hologram was used as out coupler (16). In (17) an integrated waveguide display system consisting of an infrared volume holographic grating (IVHG) and a visible light grating were recorded on the same waveguide and Gu et. al. developed a laminated composite polarizing volume grating (LCOM-PVG) (18). Shen et al have recently implemented an RGB display using coupler VHOEs (19). Blanche et al have used a system based on coupler-HOEs to extend the viewer eye box via multiple TIRs (total internal reflection) for both planar (20) and curved (21) displays.

Holography: Advances and Modern Trends VIII, edited by Antonio Fimia, Miroslav Hrabovský, Proc. of SPIE Vol. 12574, 125740E
© 2023 SPIE · 0277-786X · doi: 10.1117/12.2665596

VHOEs have also long been considered an attractive option for use in conjunction with photovoltaic (PV) devices in solar energy collection, more recently in spectrum splitting holographic solar concentrators and multiplexed systems (22), (23),(24),(25), (26). Muller et al. developed a holographic system for daylighting, solar shading and PV power generation. (27). VHOEs can act as a deflectors and/or concentrators, increasing the solar collection angle of the PV cell and improving efficiency and/or lowering costs (28). Prism Solar Technology recently patented solar concentrator systems using transmission and reflection HOEs (29) ,(30). These VHOEs can be fabricated in lightweight polymer films via light-induced refractive index modulation of the photosensitive layers which occurs due to polymerization and diffusion of monomers within the layer (31),(32). Key parameters that affect the final diffraction efficiency of VHOEs are the layer thickness, the exposure intensity and energy used, the ratio between the energies of the object and reference beams, the dark reaction time (time between recording and curing) and the spatial frequency (32), (33), (34).

Coupler-HOEs have a broad range of applications since they are designed to deflect light that would otherwise be transmitted through a film or layer and trap it through total internal reflection.

The most straightforward way to holographically record any diffractive optical element is to use a pair of recording beams with a wavelength and incident angles identical to the wavelength and beam angles at which the element will function. Coupler elements, however, present a particular challenge, since one of the beams is by design, trapped within the medium. Arranging the two recording beams to enter the medium and overlap appropriately therefore requires the use of prisms and index matching (35). While this is readily achievable in a laboratory setting, it imposes much larger challenges in mass production, mainly because of the need to avoid an air gap, and is not suitable for any kind of non-contact master-copying automated production method.

An alternative approach is to determine the slant and spatial frequency of the grating needed to diffract the input beam appropriately at the desired wavelength, then use a different recording wavelength to record that structure. With careful design, this approach can exploit the change in Bragg angle with wavelength so that the desired structure can be holographically recorded at beam angles that don't require the use of prisms. Several researchers have demonstrated this approach with success (24),(36),(37) usually for situations where one of the beams is required to be normally incident, which reduces the design complexity. Gallego et al. (38) recently demonstrated this approach for couplers designed for 633nm use, carrying out the holographic recording at green wavelengths and pointing out that different combinations of spatial frequency and slant can be used to achieve coupling in the final device. The authors demonstrate three examples, two with normal incidence and one with slightly off-normal incidence. They demonstrate the approach in three different materials which are more or less suited to different combinations of slant and spatial frequency.

The authors recently developed a model for the holographic recording of couplers of non-normally incident light, with a view to exploitation of this approach for a wide range of incidence angles and tested it for one coupler type achieving agreement of the incident and diffracted beam directions with the model predictions to a precision of ±1° and demonstrating coupling at 633nm with a diffraction efficiency up to 72 % (39).

This paper presents experimental data that is used to further test the recently developed model, which is useful for the holographic recording of diffractive optical elements designed for any input and output beam angle. It facilitates recording at wavelengths different from the operating wavelength, in order to record structures that would be otherwise be challenging or impossible to record (at the operating wavelength). It allows an at-a-glance assessment of the range of recording wavelengths that will be practical for that particular element and compensation for the effect of large beam angles on pattern contrast. It also provides data for diffraction at a range of wavelengths.

2.1 Identification of HOE parameters for desired input and output angles

The ability of a HOE to redirect an incident beam of specified wavelength at a desired angle depends primarily on two grating parameters: the spatial period and slant angle of the grating fringes. A primary objective of this simple model is to allow a user to compute the required spatial period and slant angle combination which will enable redirection of an incident beam from its initial angle (i.e., model input angle, θ_1) to another desired angle (i.e., model output angle, θ_2). Input and output angles are defined with respect to the normal of the air/glass boundary. n the simplest case, the desired HOE

structure is a uniform, volume diffraction grating characterized by a single spatial period and fringe slant angle, which obeys Bragg's Law:

$$2n\Lambda sin(\theta_B) = m\lambda \qquad \text{.....(1)}$$

where n is the refractive index of the medium, Λ is the grating period, θ_B is the Bragg angle within that medium, λ is the wavelength of the light in air, and m is the order of the diffraction. Spatial frequency in lines/mm is given by $1000/\Lambda$.
The first step is to calculate the required grating spatial period, Λ. As can be seen from figure 1, the required Bragg angle, θ_B, for the volume diffraction grating is given by

$$2\theta_B = (\theta_2 - \theta_1) \qquad (2)$$

since this is the angle through which an incident beam will be diffracted when it interacts with the grating. Thus, for any incident beam of a specified wavelength, and knowing the material refractive index (n), we can use equation 1 to determine the value of the grating spatial period, Λ, that is required for any specified values of θ_1 and θ_2.
Next, the required slant angle must be determined, which defines the orientation of the fringes relative to the material boundaries. θ_S is used to define the angle the grating planes make with the normal of the glass surface. In order to produce a specific diffracted beam making an angle θ_2 with the normal, from a beam incident at an angle θ_1, the planes of the grating need to be oriented correctly at a slant of θ_S , where

$$\theta_S = (\theta_2 + \theta_1)/2. \qquad (3)$$

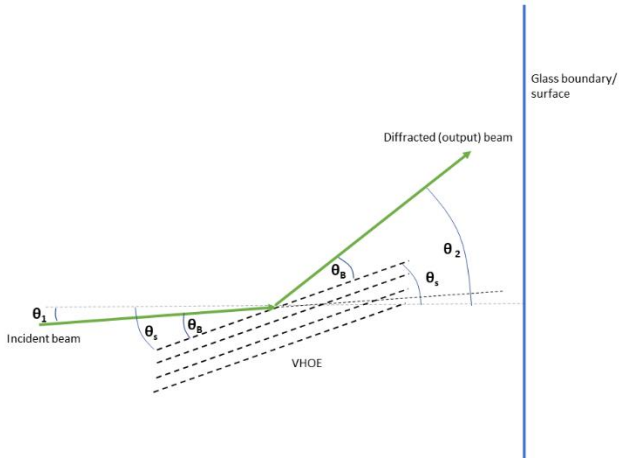

Figure 1. General relation of grating slant angle (θ_S) with incident beam angle (θ_1), Bragg angle(θ_B)and diffraction beam angle (θ_2) (all angles are within medium)

2.2. Calculation of the appropriate recording beam angles for a range of recording wavelengths

Having defined the required HOE structure (within the medium) in terms of slant angle and spatial period it is now possible to explore the range of holographic recording arrangements that could produce that slant and spatial period inside a photosensitive medium, by using different combinations of recording wavelength and recording angles. Holographic recording is achieved by overlapping two coherent beams to produce an interference pattern that has the required spatial period and slant. If the wavelength at which the HOE is deigned to function and the recording wavelength are the same, then the recording beam angles will be exactly θ_1 and θ_2 as above. The slant angle is the mean of the recording beam angles. Equation 1 is again used, but this time with the wavelength and spacing are fixed, so that the required recording angle can

be determined. We can then calculate the exact recording angles needed for that recording wavelength, inside the medium, and then the equivalent angles in air.
It should be borne in mind that for volume gratings Bragg's law (equation 1) only determines the incident and diffracted beam angles that give maximum diffraction. For beams that deviate from this, Kogelnik Coupled Wave Theory (KCWT) (40) can be used to determine the relative efficiency with which they will be diffracted, in the case that just one diffracted order propagates. Another aspect of design is matching the selectivity to a desired application. For example, high spatial frequency and thick gratings are preferable for applications involving RGB wavelength multiplexing in order to ensure minimized crosstalk, whereas the opposite is true in solar collection, where high efficiency over the broadest possible angular and wavelength range is key.

In order to achieve total internal reflection (TIR) of the diffracted beam in a typical glass or polymer medium, the incident beam angle at the internal boundary must be greater than the critical angle (e.g., 41.6˚ for a medium refractive index of 1.505). In this study, in order to achieve TIR and coupling of light inside the medium, we have specified the desired output angle of the HOE coupler device to be 45˚inside the medium, but any angle greater than the critical angle would also trap the light successfully. A more detailed description of the calculation is given in (39).

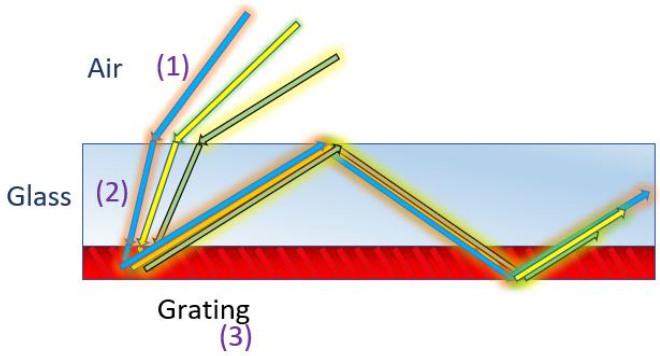

Figure 2. Principle of operation of a HOE coupler: (1) incident light beams from different angles (represented here as beams with distinct colours) enter the glass layer and are refracted; (2) the beams then enter the refractive-index matched diffraction grating and are diffracted by the grating at an angle greater than the critical angle; (3) the beams are totally internally reflected and 'coupled' along the length of the device (the precise orientation of the fringes will change for each grating.)

Figure (3a) shows the recording angles required for four HOEs designed for three different input beam angles (-40˚, -45˚ and -50° in air) for operation at 633nm wavelength and an output angle of +45° inside the medium. The curves show the recording angles needed to holographically record the required structures at a range of wavelengths. The two recording beams that need to interfere are shown in a single colour for each HOE. As would be expected, at some recording wavelengths there is no second beam, indicating that it is not possible to achieve the required angle in air (without use of prisms). It is possible to examine the graph and quickly decide on recording wavelengths for which there are corresponding achievable recording angles, bearing in mind practical difficulties with reflection and obliquity losses at very high angles of incidence, as well as any particular material considerations such as avoidance of very high slant angles. Figure (3b) shows the linear variation of slant angle inside the medium along with the three different incidence angles in air.

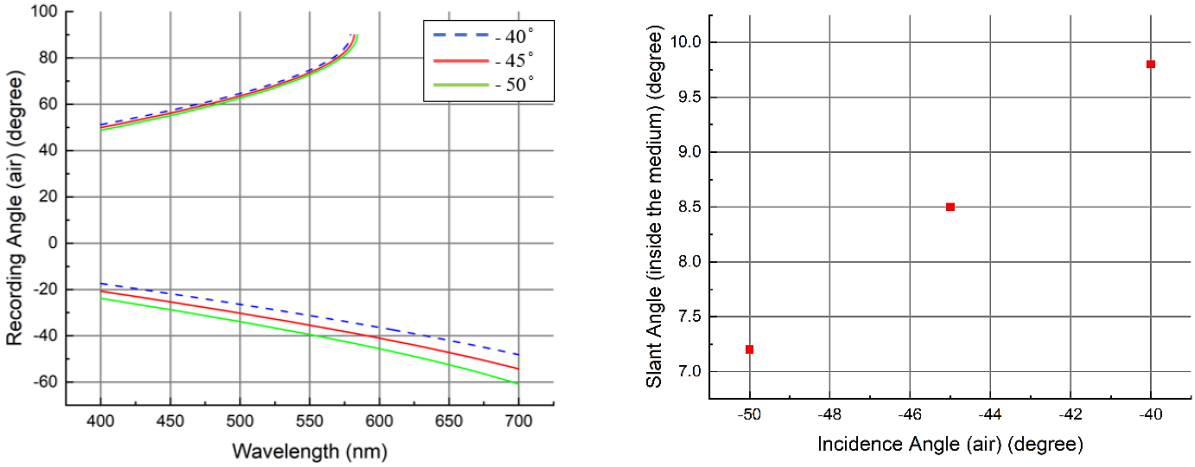

(a) (b)

Figure 3. (a) Recording angles for both recording beams (in air) v/s. recording wavelength for three HOE couplers designed for 633nm with an incident angle (in air) of -40˚, -45˚and -50˚(b) Slant angle for each of the three HOE couplers. In all cases the slant angle is such that the 633nm beam is diffracted internally at +45˚and thus is totally internally reflected.

In this study, we have chosen three input beam angles -40˚, -45˚and -50˚in air. Table 1 shows the spatial frequency and slant of the structure necessary for each VHOE as well as the angles of the beams needed to record that structure using 532nm light. For example, to produce the desired +45˚output angle in the medium, and an input beam angle of -40˚in air for a specified wavelength of 633 nm, the required slant angle is 9.8° inside the medium and the required spatial frequency is 2737 lines/mm). The recording angles to record that structure with a 532 nm laser are -29.4˚and 70.5˚outside the medium. The inter-beam angles for each case are given in table-1.
Figure 4 shows example of couplers designed for use at 633nm, holographically recorded by the interference of two green laser beams for the three different recording conditions. In order to combat the losses due to high angles of incidence, the obliquity factor is considered in the design. The losses due to Fresnel reflection at the air-photopolymer interface are also considered in the model.

Table 1: Conditions 532nm recording for three different HOE Couplers designed to operate at 633nm

633 nm	**Recording at 532 nm**				
Desired angle of incidence (Degrees, in air)	**Recording Beam 1** (Degrees, in air)	**Recording Beam 2** (Degrees, in air)	**Total Inter-beam angle** (Degrees, in air)	**Slant Angle** (Degrees, inside medium)	**Spatial Frequency** (lines/mm)
-40	-29.4	70.5	99.9	9.8	2737
-45	-33.5	69.5	103	8.5	2829
-50	-37.4	68.5	105.9	7.2	2914

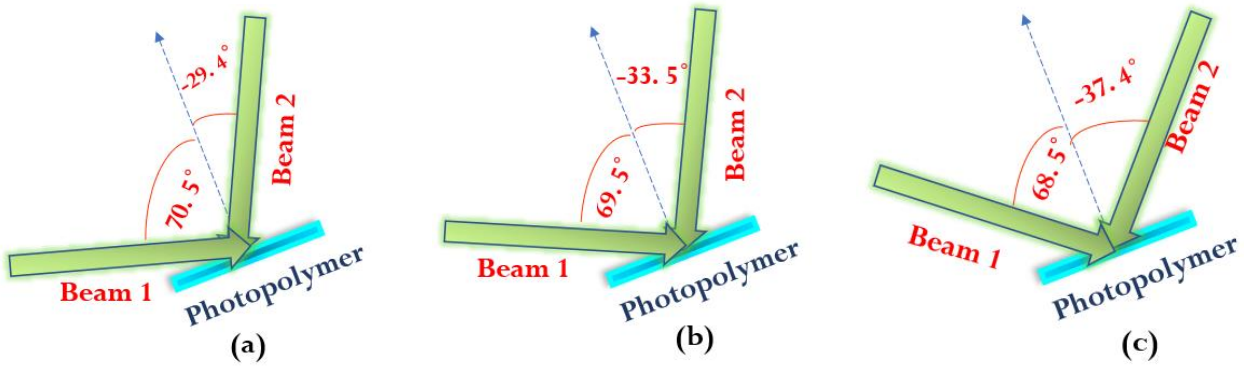

Figure 4. Recording beams of 532nm (green arrows) needed for a grating designed to work as a coupler of input angles (a)-40° (in air) (b) -45° (in air) and (c) -50° (in air) at 633nm. All angles here are outside the medium.

2.3. Modelling the two incident angles at which Bragg diffraction peaks for a range of input beam wavelengths:

To characterize the performance of the couplers, their diffraction efficiency is measured over a range of incident angles with the wavelength fixed at 633nm and also at a range of wavelengths with the incident angle fixed for each measurement. In order to facilitate data analysis, the model had also been adapted so that it can predict the incident angles at which the Bragg diffraction peaks will appear for a range of input beam wavelengths for a specific recorded grating. In this version, the recording arrangement and wavelength are the inputs and the model calculates the expected Bragg peak positions using the steps outlined in authors previous paper (39). Since the photonic structures are designed to work as couplers for a wavelength of 633nm,there is only one Bragg diffraction peak at 633nm.

Figure 5 shows the calculated angle of incidence for maximum Bragg diffraction (in air) from the recorded grating structures modelled at a range of test wavlengths. This is plotted as a function of incident beam wavelength over the visible range.

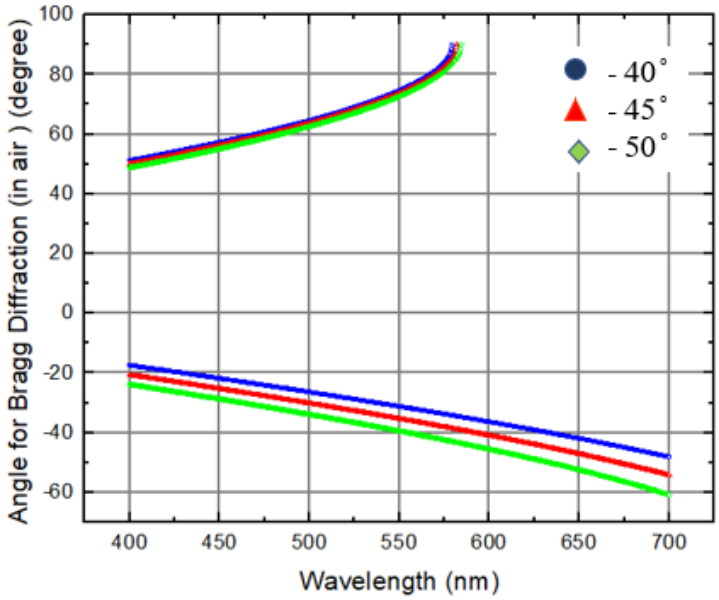

Figure 5. Expected incident beam angles for maximum Bragg diffraction v/s wavelength for the HOE couplers (HOE Coupler 1-designed for input angle -40° in air and output angle 45 °in the medium (633nm), HOE Coupler2- designed for input angle -45 ° in air and output angle 45 °in the medium (633nm), HOE Coupler 3- designed for input angle -50 ° in air and output angle +45 °in the medium (633nm)).

3. FABRICATION AND TESTING OF VHOEs – MATERIALS AND METHOD

3.1. Fabrication of VHOEs

Following identification of the recording beam angles required to produce holographic couplers with the desired input and output angles using the theoretical model, a set of coupler devices were fabricated in order to further test the theoretical model. A commercially-available Bayfol HX 200 photopolymer film was used, which is sensitive to red, green and blue wavelengths (41). The Bayfol HX 200 layer has a thickness of 16 ± 2 µm and a refractive index modulation greater than 0.03 can be achieved. To ensure sufficient stability during holographic recording, the Bayfol HX 200 film was laminated onto a glass slide. Holographic recording was conducted using a two–beam interferometric geometry as shown in Figure 6(a). Briefly, a single 532nm beam from a (Cobolt Samba™ 1500 532nm) laser was directed through a half wave plate, spatially filtered and collimated, before division by a beam splitter cube. Using a two-mirror arrangement, the two recording beams were redirected to overlap at the photosensitive layer. The mirror as shown in fig. 6(a) is rotated in three different positions to get three different inter-beam angles (as per Table 1) to record three different HOE Couplers. The laser beam intensity was monitored using an optical power meter (Newport, model 843-R), and data was transferred to a computer. The holographic recording exposure time was controlled via an electronic shutter. The total exposure energy (mJ/cm^2) is estimated from Intensity (mW/cm^2) x Exposure time (s). Coupler Diffraction Efficiency (CDE) is calculated as the percentage of the available light intensity that is diverted into TIR-trapped light within the glass medium.
The influence of the recording conditions (recording intensity, exposure energy) on the efficiency of the coupler devices fabricated in the Bayfol HX 200 film was investigated, and the results are presented in section 4.1. It is important to restate that obliquity and Fresnel reflection losses were accounted for in all calculations of total recording intensity. Table 2 below shows the computed intensities which are required in beam 1 and beam 2 in order to yield the total intensity desired inside the film/medium.

Table 2: Recording intensities for the beams incident of the photopolymer calculated to compensate for reflection losses and obliquity at the recording angles, for HOEs designed for -40˚, -45˚and -50˚ incidence angles in air diffracted to +45˚ angle inside the medium (for 633nm operating wavelength).

633 nm	**Recording at 532nm**				
Angle of incidence (Degrees, in air)	**Angle Beam 1** (Degrees, in air)	**Angle Beam 2** (Degrees, in air)	**Intensity Beam 1,** (mW/cm^2, in air)	**Intensity Beam 2,** (mW/cm^2, in air)	**Intensity beam ratio** (in medium).
-40	-29.4	70.5	0.53	2.71	1:1
-45	-33.5	69.5	1.33	6.23	1:1
-50	-37.4	68.5	0.53	1.88	1:1

3.2. Characterization of VHOE performance

In the Bragg analysis setup, the fabricated holographic coupler was positioned on an electronically-controlled rotational stage (Newport ESP300). The couplers were probed by a 633 nm He-Ne laser (Uniphase™ 106-1) and it was ensured that when the probe beam is normal to the sample, the reading on the rotation stage corresponds to 0 degrees. For each case, the intensity of the transmitted beam was measured and the percentage trasmitted in the zero-order beam is cacluated based

on an initial intensity transmitted though glass, which is taken as 100% transmission and equivalent to 0% diffraction into any other beam. The coupler diffraction efficiency (CDE) is calculated using the following method

$$\text{CDE}= \frac{(Background\ level\ of\ \%\ transmission)-(\%\ transmission\ at\ Bragg)}{(Background\ level\ of\ \%\ transmission)} \quad ..(4)$$

By rotating the coupler via the stage, wide angle transmission efficiency scans were obtained. This allowed for identification and positional measurement of the reconstructed diffraction peaks and the results are presented in section 4.2. A full angular scan was also completed with a glass slide to allow esitimation of reflection losses. Furthermore, the interaction of the gratings with white light has been studied. For this purpose, they have been placed in front of broadband light source (Avalight-HAL-S-mini) and the transmission spectra recorded for a range of angles of incidence on the VHOE couplers (around the design angle) using a UV-Vis spectrophotometer (Avantes AvaSpec-2048-SPU).

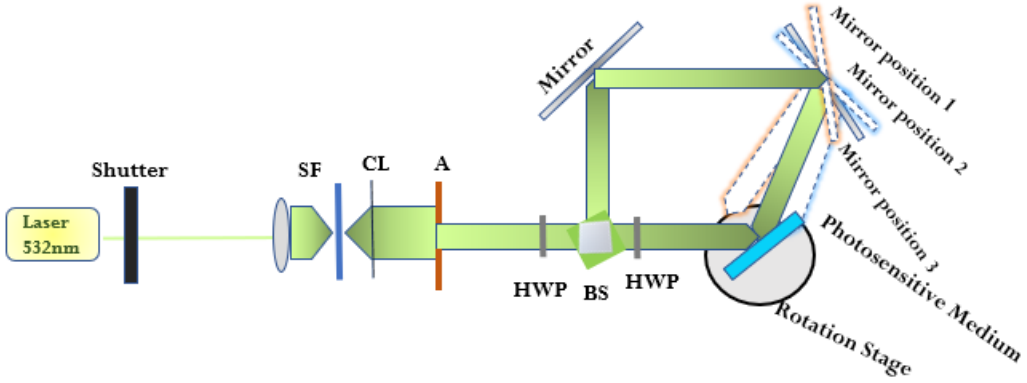

(a)

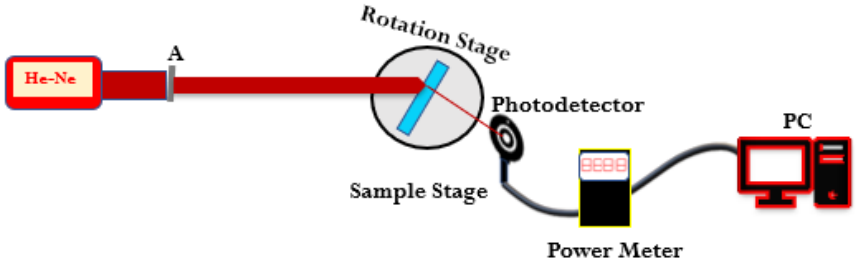

(b)

Figure 6. (a) Recording set-up and (b)Characterization set-up for the VHOE couplers

4. EXPERIMENTAL RESULTS

4.1. Optimization of the holographic recording conditions for couplers

Using the recording arrangement described in section 3.1, couplers were recorded holographically with 532nm light for a range of exposure conditions and their diffraction efficiencies was measured as per section 3.2. Figure 7 (a) shows the coupler diffraction efficiency (measured at 633nm) for different exposure times for each of the three VHOEs recorded with 532nm and total intensity inside the medium of 1mW/cm^2 (for -40˚ and -50˚ input angles in 633nm) and 2mW/cm^2 (for -45˚ input angle in 633nm). From Figure 7(a) we can conclude that highly efficient couplers are readily achievable at a range of exposure conditions. The minimum exposure energy required for efficiency above 60% appears to be approximately 7-10mJ/cm^2 which is compatible with mass production requirements. Efficiency of 70% was achieved with approximately 10 seconds of exposure at 2mW/cm^2. At longer times and higher exposure energies the data is quite scattered but broadly in the 60-70% range, and not significantly increased or decreased by further exposure. We expect that this is due to the well-designed maximum refractive index modulation and thickness of the Bayfol HX 200 photopolymer layers. Repeatability of the experiment can be seen from figure 7 (b), where a specific example of couplers of -40˚ input angle (in air) in 633nm with different exposure times is shown. While the CDE of the intended diffraction peaks varies in the range of 50-70% for the different exposure times as expected, the angular positions of the diffraction peaks are highly repeatable. Characterization of the peak positions is discussed further in sections 4.2 and 4.3.

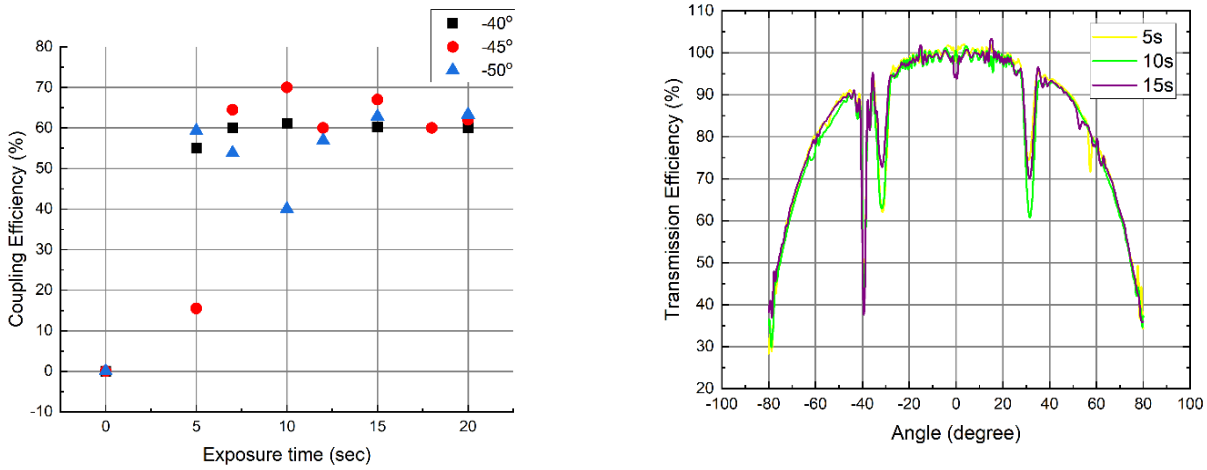

(a) **(b)**

Figure 7. (a) Coupler diffraction efficiency at 633nm v/s exposure time for three different types of HOE Coupler :. -40˚, -45˚ and -50˚ input angles. All angles are in air. (b) Transmission efficiency v/s angle for -40˚ HOE Coupler (in air) at 633nm for different exposure times.

4.2. Diffraction characteristics at a range of angles of incidence.

In order to examine the diffraction behavior of the recorded photonic structure for 633nm light in more detail wide-angle zero-order Bragg curves were measured at 633 nm. Figure 8 (a) shows the wide-angle angular scans for three different HOE couplers designed to have three different input angles of incidence. Green, red and blue curves show the transmission efficiency v/s angle for angle of incidence of -40˚ (in air), -45˚ (in air) and -50˚ (in air) respectively. Figure 8 (b) shows a magnified section showing the intended coupler diffraction peaks in greater detail. It should be noted that for Figure 8(a) and (b) an FFT filter is used to smooth the curve.

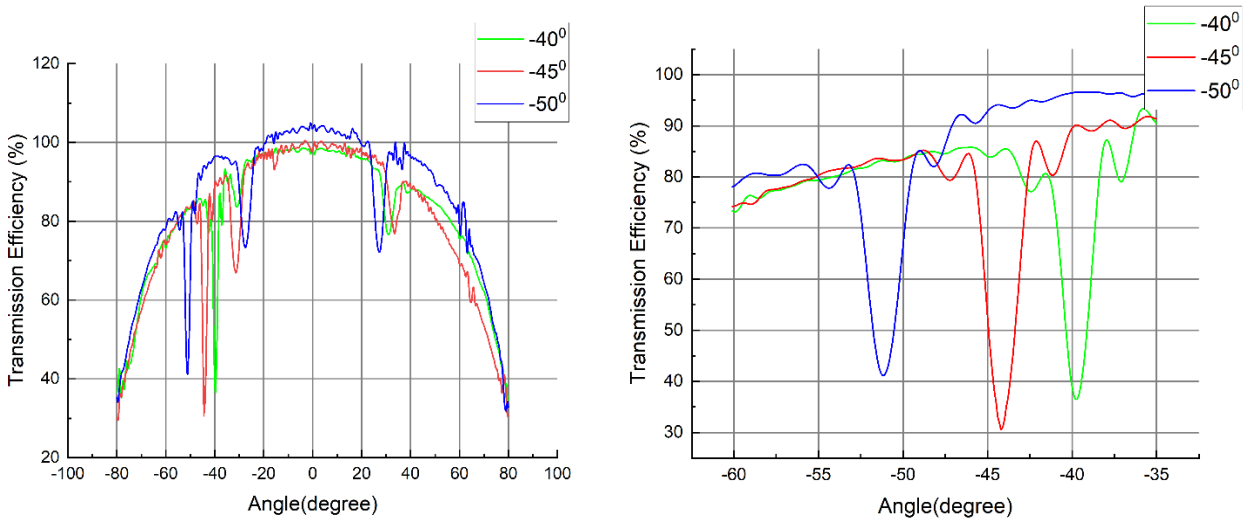

Figure 8. (a) Wide angle transmission efficiency versus angle of incidence for the HOE couplers when probed with 633nm, (b) Magnified figure of the coupler diffraction peaks of interest.

Three different angles for maximum Bragg diffraction are observed for the three HOE couplers tested and they are relatively well matched to the intended angles of incidence. As can be seen from Figure 2(b) there is a match of peak position to within ±1.5° (in air) with the HOE coupler designed for 50° having the largest deviation. As was seen in Figure 7(b), the repeatability within one recording arrangement is improved further. The standard deviation on the peak position for all the samples of -40˚(in air) from figure 7(b) is ± 0.19˚. The equivalent data for the -45˚and -50˚recordings have standard deviations ± 0.50˚and ± 0.11˚respectively as shown in Table 3.

Table 3 shows the model-predicted angles (in air) and measured angles (in air) for three different HOE Couplers.

Expected Angle (Degrees, in air)	**Mean Value of the Measured Angles (Degrees, in air)**	**Standard Deviation of the Measured Angles (Degrees, in air)**
-40.0	-39.5	0.19
-45.0	-44.0	0.50
-50.0	-51.1	0.11

The experimental error on setting the recording beam angles is estimated at ±0.2˚, while the error on setting the photopolymer layer in the holder for recording is estimated at ±0.3˚and the error that arises in estimating the position of maximum diffraction on the angular scans is estimated at approximately ±0.1˚. In this context, and bearing in mind that there will inevitably be some material issues contributing (small amounts of shrinkage etc), the experimental data is considered to be well matched to the model, validating the approach. The maximum coupling efficiency at the design wavelength of 70% is achieved from coupler recorded with total intensity of 2mW/cm^2 and exposure time of 10s.

4.3. Diffraction characteristics at a range of wavlengths.

The diffraction peaks obtained with a broadband white light source were also studied using a UV-Vis spectrophotometer. Figure 9(a-c) plots all of the peaks observed in the spectrum for the incident angles used to obtain the spectrum, for each of the three VHOE Couplers (-40˚,-45˚and -50˚). An example of one of the sets of spectra from which this data was obtained is shown in figure 9(d). In all of the HOE couplers, peaks were observed at the angles and wavelengths expected

for that coupler. For example, the blue line in 9(d) represents the data for a 40° angle of incidence and so would be expected to have a peak at 633nm (the design wavelength) which is indeed visible in the spectrum. For the plots in Figure 9(a-c) the appropriate theoretical curve from Figure 5 has been included in order to show the angles where diffraction would be expected for each wavelength. This agreement is further confirmation of the model and demonstration of an ability to control the HOE coupler design. However, as is obvious from the plots in figure 9, there were also many additional peaks noted. In most cases the strongest peaks corresponded to the modelled data. The additional (unwanted) peaks were not randomly located in the plots but formed two distinct lines as the peak position shifted with the angle of incidence. These are very likely to be due to spurious gratings, which can also be seen in the angular scans in figure 8, as diffraction occurring (near +30° and -30°) in the 633nm angular scans. As discussed in the authors previous work, it is relatively straightforward to identify the source of spurious gratings when data for the Bragg peaks is available at a number of different wavelengths. For example, the peak positions for one of the sets in Figure 9(b) is a close match for the diffraction from the spurious grating modelled in reference (39), Figure 12(b), which is caused by the back reflection of the 69.5° recording beam interfering with the beam itself.

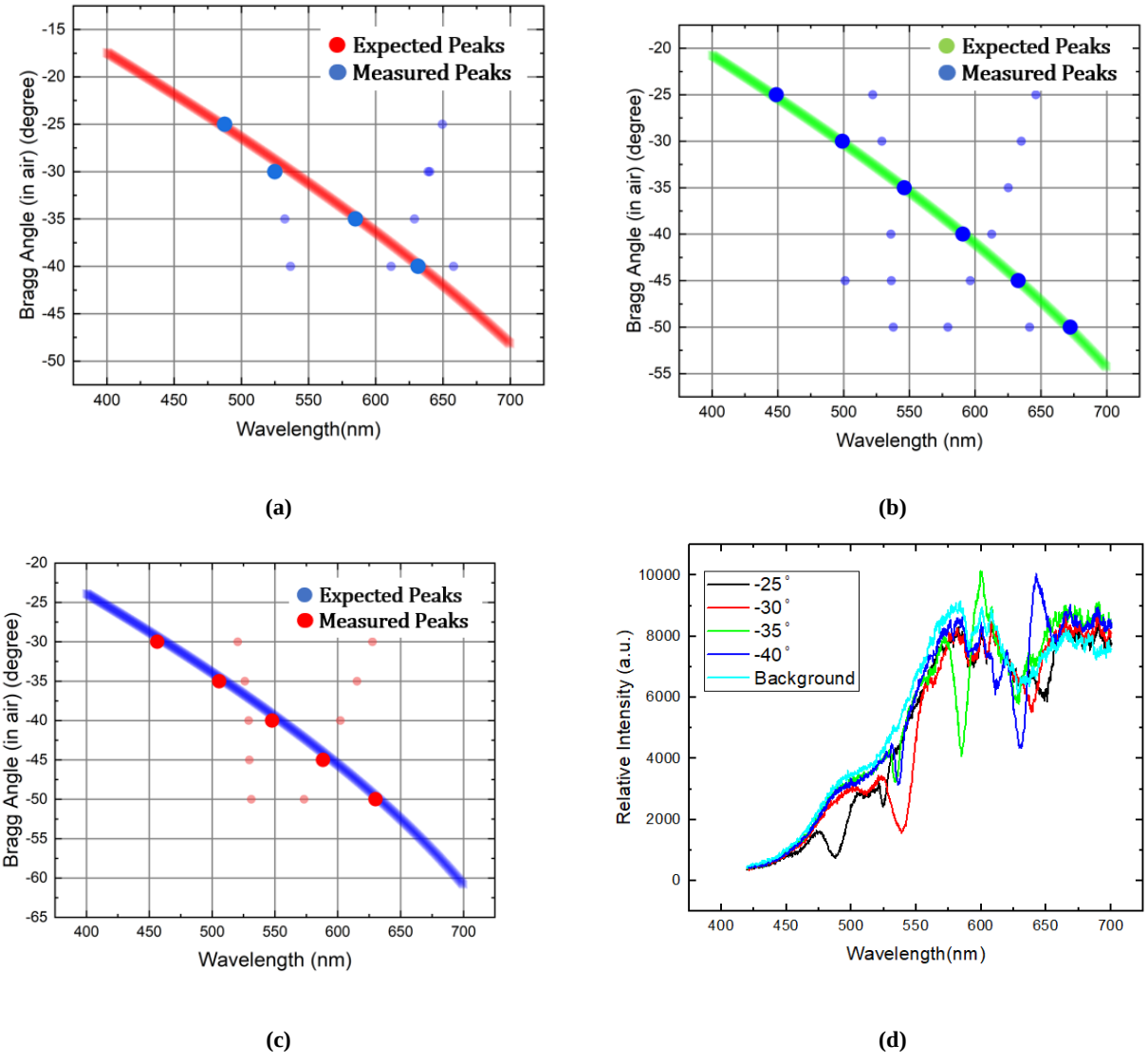

Figure 9. Expected peaks and measured peaks obtained from UV- Vis spectrophotometer for (a) input angle -40° in air and output angle +45 °in the medium (633nm) (b) input angle -45° in air and output angle +45 °in the medium (633nm) (c) input angle -50° in air and output angle +45 °in the medium (633nm).(d) shows the results from UV-Vis spectrophotometer for different incidence angles in air for the VHOE Coupler having input angle -40° in air and output angle +45 °in the medium (633nm).

5. DISCUSSION

The objective of this experimental study was to further investigate the validity of a theoretical model for the use in the design and fabrication of VHOE couplers, recently reported in (39). This previous study included detailed experimental characterization of a VHOE coupler designed for operation at a single input angle (-45º). Here, we have extended this study to three coupler input angles: -40˚, -45˚ and -50˚, with a view to testing the wider applicability of the approach. First, the grating period, slant angle and recording beam angles required to fabricate these couplers were identified using the theoretical model (Table 1). After accounting for obliquity factors and reflection losses, the couplers were experimentally fabricated in a commercially available Bayfol photopolymer and characterized at the intended coupler operational wavelength of 633 nm.

There are a number of observations that can be drawn from the characterization data shown above. Firstly, the fabricated couplers do indeed function as intended. A comparison of the expected and experimentally measured diffraction angles for each coupler is shown in Table 3. The mean value of measured diffraction peaks are within ±1.5° (in air) of the expected value for all the examples demonstrated above. No second diffraction peak is expected in Figure 8(b) because the scan is performed by varying the incidence angle in air, and at this wavelength the HOE functions as a coupler and therefore the second angle of incidence that would produce strong diffraction is impossible to access from outside the air/glass boundary. We have observed a few spurious grating peaks in this study, as seen in Figures 8 and 9. The origin of such peaks is similar to our previous study, and is discussed in detail in (39).

6. CONCLUSION

In this study we have used a previously developed theoretical model which enables design of HOE couplers for different incidence angles. This model was used to aid the fabrication of VHOE couplers for operation at 633 nm using a recording wavelength of 532 nm for three different incident angles. Different recording exposure times for three different inter-beam angles were investigated for the fabrication of high efficiency couplers. We recorded HOE couplers of -40˚, -45˚and -50˚ input angles (in air) and output angle of +45˚(in medium) in 633 nm and we obtained a maximum diffraction efficiency of 70 %. Couplers designed for incident angles of 40°, -45˚and -50˚were observed to have maximum diffraction which agreed to within ±1.5°, in air, with expected angles for a coupler operational wavelength of 633nm. Good agreement was also found when the HOE couplers were probed with white light.

7. AUTHOR CONTRIBUTIONS

SM VT and IN developed the initial concept; SM and DCH obtained the funding for the project; SM led the project; SM, DCo and DCh contributed to the experimental plan for this manuscript and provided supervision; SM developed the model and DCh implemented it in MATLAB. DCh carried out most of the experimental work with help from RG, SA and SM. SM, DCo and DCh contributed to the data analysis; DCh produced most of the Figures; DCh wrote the initial manuscript draft; All authors edited the manuscript.

8. FUNDING

Dipanjan Chakraborty is funded by Technological University Dublin Research Scholarship programme. Rosen Georgiev and Suzanne Martin received funding from Enterprise Ireland and the European Union's Horizon 2021 Research and Innovation Programme under the Marie Skłodowska-Curie grant agreement No. 847402. All authors thank FOCAS, TU Dublin for the provided technical facilities and administrative support.

9. CONFLICTS OF INTEREST

The authors declare no conflict of interest.

REFERENCES

1. Ashley J, Bernal M-P, Burr GW, Coufal H, Guenther H, Hoffnagle JA, et al. Holographic data storage technology. IBM journal of research and development. 2000;44(3):341-68.
2. Dhar L, Hill A, Curtis K, Wilson W, Ayres M. Holographic data storage: from theory to practical systems: John Wiley & Sons; 2011.
3. Li J, Hu P, Jin J, Wang J, Liu J, Wu J, et al. Highly sensitive photopolymer for holographic data storage. Optics Express. 2022;30(22):40599-610.
4. Miller JM, de Beaucoudrey N, Chavel P, Turunen J, Cambril E. Design and fabrication of binary slanted surface-relief gratings for a planar optical interconnection. Applied optics. 1997;36(23):5717-27.
5. Soares O. Holographic coupler for fiber optics. Optical Engineering. 1981;20(5):740-5.
6. Singh AK, Yadav A, Khan AA, Roy S, Yadav HL. Design and analysis of holographic optical elements for their use as couplers with appreciable efficiency at different optical transmission windows. Optik. 2022;261:169184.
7. He C, Neild A, Helmerson K, Cincotta S, Zuk J, Armstrong J. Dual-aperture hologram receiver for visible light communications. Optics Communications. 2021;490:126943.
8. Shimizu S, Okamoto A, Mizukawa F, Ogawa K, Tomita A, Takahata T, et al. Volume holographic spatial mode demultiplexer with a dual-wavelength method. Applied Optics. 2018;57(2):146-53.
9. Zhang Y, Fan H, Poon T-C. Optical image processing using acousto-optic modulators as programmable volume holograms: a review. Chinese Optics Letters. 2022;20(2):021101.
10. Alcaraz PE, Nero G, Blanche P-A. Bandwidth optimization for the Advanced Volume Holographic Filter. Optics Express. 2022;30(1):576-87.
11. Park J-H, Lee B. Holographic techniques for augmented reality and virtual reality near-eye displays. Light: Advanced Manufacturing. 2022;3(1):1-14.
12. Putilin A, Morozov A, Kopenkin S, Dubynin S, Borodin YP. Holographic waveguide periscopes in augmented reality displays. Optics and Spectroscopy. 2020;128(11):1828-36.
13. Li G, Lee D, Jeong Y, Cho J, Lee B. Holographic display for see-through augmented reality using mirror-lens holographic optical element. Opt Lett. 2016;41(11):2486-9.
14. Piao J-A, Li G, Piao M-L, Kim N. Full Color Holographic Optical Element Fabrication for Waveguide-type Head Mounted Display Using Photopolymer. J Opt Soc Korea. 2013;17(3):242-8.
15. Wu Z, Liu J, Wang Y. A high-efficiency holographic waveguide display system with a prism in-coupler. Journal of the Society for Information Display. 2013;21(12):524-8.
16. Zhang N, Liu J, Han J, Li X, Yang F, Wang X, et al. Improved holographic waveguide display system. Appl Opt. 2015;54(12):3645-9.
17. Lv Z, Liu J, Xiao J, Kuang Y. Integrated holographic waveguide display system with a common optical path for visible and infrared light. Opt Express. 2018;26(25):32802-11.
18. Gu Y, Weng Y, Wei R, Shen Z, Wang C, Zhang L, et al. Holographic waveguide display with large field of view and high light efficiency based on polarized volume holographic grating. IEEE Photonics Journal. 2021;14(1):1-7.
19. Shen Z, Wang C, Weng Y, Zhang Y, editors. 15.2: Design and Realization of Full-Color VHG Holographic Waveguide Display. SID Symposium Digest of Technical Papers; 2022: Wiley Online Library.
20. Draper CT, Bigler CM, Mann MS, Sarma K, Blanche P-A. Holographic waveguide head-up display with 2-D pupil expansion and longitudinal image magnification. Applied optics. 2019;58(5):A251-A7.
21. Draper CT, Blanche P-A. Holographic curved waveguide combiner for HUD/AR with 1-D pupil expansion. Optics Express. 2022;30(2):2503-16.
22. Collados MV, Chemisana D, Atencia J. Holographic solar energy systems: The role of optical elements. Renewable and Sustainable Energy Reviews. 2016;59:130-40.
23. Kostuk RK, Rosenberg G, editors. Analysis and design of holographic solar concentrators. High and Low Concentration for Solar Electric Applications III; 2008: International Society for Optics and Photonics.
24. Naydenova I, Akbari H, Dalton C. M. Yahya so M. Ilyas, C. Pang Tee Wei, V. Toal, S. Martin, Photopolymer Holographic Optical Elements for Application in Solar Energy Concentrators. Holography-Basic Principles and Contemporary Applications, E Mihaylova (Ed), InTech. 2013.

25. Zhang D, Gordon M, Russo JM, Vorndran SD, Kostuk RK. Spectrum-splitting photovoltaic system using transmission holographic lenses. Journal of Photonics for Energy. 2013;3(1):034597.
26. Ferrara MA, Bianco G, Borbone F, Centore R, Striano V, Coppola G. Volume holographic optical elements as solar concentrators. Holographic Materials and Optical Systems. 2017:27-50.
27. Müller H. Application of holographic optical elements in buildings for various purposes like daylighting, solar shading and photovoltaic power generation. Renewable Energy. 1994;5(5-8):935-41.
28. Neipp C, Taleb SI, Francés J, Fernández R, Puerto D, Calzado EM, et al. Analysis of the Imaging Characteristics of Holographic Waveguides Recorded in Photopolymers. Polymers. 2020;12(7):1485.
29. Aspnes ED, Castillo-Aguilella JE, Courreges RD, Hauser PS, Stewart KR. Non-latitude and vertically mounted solar energy concentrators. Google Patents; 2013.
30. Aspnes ED, Castillo-Aguilella JE, Courreges RD, Hauser PS, Stewart KR. Solar energy concentrator with multiplexed diffraction gratings. Google Patents; 2013.
31. Kao H, Ma J, Wang C, Wu T, Su P. Crosstalk-Reduced Double-Layer Half-Divided Volume Holographic Concentrator for Solar Energy Concentration. Sensors. 2020;20(23):6903.
32. Huang Q, Ashley PR. Holographic Bragg grating input–output couplers for polymer waveguides at an 850-nm wavelength. Applied optics. 1997;36(6):1198-203.
33. Wang C, Ma J, Kao H, Wu T, Su P. Wide-Band High Concentration-Ratio Volume-Holographic Grating for Solar Concentration. Sensors. 2020;20(21):6080.
34. Ludman JE. Holographic solar concentrator. Applied Optics. 1982;21(17):3057-8.
35. Bigler CM, Blanche P-A, Sarma K. Holographic waveguide heads-up display for longitudinal image magnification and pupil expansion. Applied optics. 2018;57(9):2007-13.
36. P. Stoeva TM, B. Rogers, M. Oubaha, S. Martin, M.A. Ferrara, G.Coppola and I. Naydenova. Photonics Ireland 14-16 June, 2021.
37. Toal V, Whelan M, Volcan A, Naydenova I, Martin S. Replay at optical communications wavelengths of holographic gratings recorded in the visible: SPIE; 2006.
38. Fernández R, Bleda S, Gallego S, Neipp C, Márquez A, Tomita Y, et al. Holographic waveguides in photopolymers. Opt Express. 2019;27(2):827-40.
39. Chakraborty D, Georgiev R, Aspell S, Toal V, Naydenova I, Cody D, et al. Modelling and Design of Holographic Optical Elements for Beam-Coupling Applications for a Range of Incident Beam Angles. Photonics. 2022;9(12):936.
40. Kogelnik H. Coupled wave theory for thick hologram gratings. Landmark Papers On Photorefractive Nonlinear Optics: World Scientific; 1995. p. 133-71.
41. Bruder F-K, Fäcke T, Rölle T. The chemistry and physics of Bayfol® HX film holographic photopolymer. Polymers. 2017;9(10):472.